Computational fluid dynamics simulation of the homogeneous flow regime in a large-scale bubble column

N Varallo*, G Besagni, R Mereu and F Inzoli

Politecnico di Milano, Department of Energy, Via Lambruschini 4a, 20156 Milano, Italy

* Corresponding author: Type the corresponding author's e-mail address here

Abstract. Bubble column reactors are used in many industrial applications, but their characterisation at both global and local scales has always been very complex. In this work, a CFD Eulerian multi-fluid approach is developed to describe the hydrodynamics of large-scale bubble columns, focusing on the homogeneous flow regime. Transient 3-D simulations have been performed employing a commercial code (ANSYS Fluent 2023 R2), considering a fixed mono and poly-dispersed bubble size distribution for modelling the dispersed gas phase. The results have been critically analyzed, and the discrepancies between the numerical and experimental results have been commented on, setting the stage for future improvements.

1. Introduction

Bubble columns are multiphase reactors widely used in the chemical, biochemical, petrochemical, food, and pharmaceutical industries because of their several advantages. They are characterized by excellent heat and mass transfer between the phases, high durability, and low operating and maintenance costs due to the absence of moving parts [1]. They are used, for example, in the Fischer-Tropsch process to produce liquid hydrocarbons and in the LOPROX process, which aims to improve the biodegradability of heavily contaminated products [2].

The simplest bubble column configuration consists of a vertical vessel with a gas distributor at the bottom, which disperses the gas phase as bubbles or coalescence-induced structures into the column. The liquid phase may be fed co-currently or counter-currently to the rising bubbles. The bubble column operates in batch mode when bubbles rise in a quiescent liquid phase.

Despite the simple column arrangement, bubble columns are characterized by extremely complex fluid dynamics interactions between the phases, manifesting in different flow regimes.

The fluid dynamics in large-scale bubble columns explicates in six flow regimes and can be described by a relation between two global flow parameters, the drift flux and the gas holdup [3].

The six flow regimes emerging upon an increase in the gas flow rate are: (1) mono-dispersed homogeneous flow regime, (2) poly-dispersed homogeneous flow regime, (3) transition flow regime without coalescence-induced structures, (4) transition flow regime with coalescence-induced structures, (5) pseudo-heterogeneous flow regime, and (6) pure heterogeneous flow regime (figure 1).

The homogeneous flow regime is observed at low superficial gas velocities, and only non-coalescence-induced bubbles characterize it. Depending on the bubble size distribution (BSD), two distinctions can be made within the homogeneous flow regime: the mono-dispersed and the poly-dispersed homogeneous flow regimes.

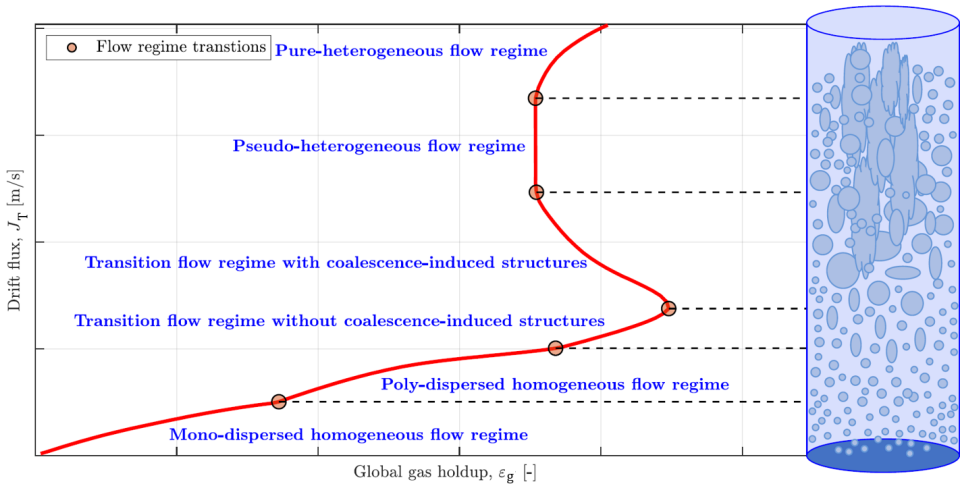

Figure 1. Bubble column operating curve. The drift flux, J_T, is defined as the volumetric flux of either components relative to a surface moving at volumetric average velocity.

The lift force sign change is pivotal for defining the transition between these flow regimes. Then the transition flow regime without coalescence induced structures begins to be established by non-stable coalescence-induced structures, which induce gas holdup oscillations and which are related to Ledinegg instabilities.

Later, structures induced by coalescence become stable, defining the transition flow regime with coalescence-induced structures. Although these coalescence-induced structures are observed in the bubble column, they are not fully formed. Indeed, as the gas flow rate increases, the gas holdup decreases, revealing an imbalance between higher gas flow rates and the development of coalescence-induced structures.

A further increase in the gas flow rate leads to the pseudo-heterogeneous flow regime, characterized by an equilibrium between the increase in the gas flow rate (in terms of drift flux) and the formation of coalescence-induced structures.

At even higher superficial gas velocities, a fully heterogeneous flow regime is attained, which is associated with elevated coalescence and breakage rates and an even larger range of bubble sizes.

This paper focuses on the mono-dispersed and poly-dispersed homogeneous flow regime and it is organized as follows. Section 2 presents the experimental benchmark used for the model validation and section 3 the model details and numerical settings. Section 4 compares the numerical results with the experimental data. Finally, conclusions are drown and avenues for future studies are proposed.

2. Experimental benchmark

The experimental data of Besagni [3] were used as a reference for this work. The experimental facility consists of a non-pressurized vertical pipe made of Plexiglas with height $h_c = 5.3$ m and inner diameter $D_c = 0.24$ m. The column was equipped with a perforated plate sparger of 581 holes of 0.5 mm.

Measurement of the bed expansion (the height of the liquid free surface when air flows in the column) allowed the evaluation of the global gas holdup and a double-fiber optical probe system was used to measure the local fluid dynamics properties (i.e., local void fraction profile). The optical probe was inserted, via an access port, into the flow at an axial position of 1.9 m from the sparger. Finally, image analysis was performed to obtain the bubble size distribution.

3. The numerical model

3.1. Governing equations

The Eulerian two-fluid approach has been used in this study. Within such a framework, the Navier-Stokes equations are ensemble-averaged, and the effect of turbulence and interphase phenomena are considered using closure models. For an isothermal flow without mass transfer, the continuity and momentum equation for the k-phase read as

$$\frac{\partial}{\partial t}(\alpha_{\mathrm{k}}\rho_{\mathrm{k}}) + \nabla \cdot (\alpha_{\mathrm{k}}\rho_{\mathrm{k}}\,\boldsymbol{u}_{\mathrm{k}}) = 0 \tag{1}$$

$$\frac{\partial}{\partial t}(\alpha_{\mathrm{k}}\rho_{\mathrm{k}}\boldsymbol{u}_{\mathrm{k}}) + \nabla \cdot (\alpha_{\mathrm{k}}\rho_{\mathrm{k}}\boldsymbol{u}_{\mathrm{k}}\boldsymbol{u}_{\mathrm{k}}) = -\alpha_{\mathrm{k}}\nabla p + \nabla \cdot (\alpha_{\mathrm{k}}\,\bar{\tau}_{\mathrm{k}}) + \alpha_{\mathrm{k}}\rho_{\mathrm{k}}\boldsymbol{g} + \boldsymbol{M}_{I,\mathrm{k}} \tag{2}$$

The right-hand side term of 2quation (2) represents the pressure gradient, the stresses (Reynolds and viscous), the body forces, and the interfacial momentum exchanges between the phases, respectively.

3.2. Interfacial momentum exchange

The interactions between the continuous and the dispersed phases are considered by a source term in the momentum equation. The last term of Equation (2) comprises several physical mechanisms: drag, lift, turbulent dispersion, wall lubrication, and virtual mass forces:

$$\boldsymbol{M}_{\mathrm{I,k}} = \boldsymbol{F}_{\mathrm{D,k}} + \boldsymbol{F}_{\mathrm{L,k}} + \boldsymbol{F}_{\mathrm{TD,k}} + \boldsymbol{F}_{\mathrm{WL,k}} + \boldsymbol{F}_{\mathrm{VM,k}} \tag{1}$$

A summary of the closure models used in this study is presented in Table 1.
Particular attention has been given to the lift force, comparing different lift coefficient correlations (figure 2), which predict a different critical bubble diameter for the change in sign of the lift coefficient.

Table 1. Summary of the closure models for the interfacial momentum exchanges used in this study.

Interfacial force	Model	Notes
Drag	Tomiyama [4]	
Lift	Tomiyama [5]	
	Ziegenhein [6]	
	Hessenkemper [7]	
Turbulent dispersion	Burns [8]	Not used in the poly-dispersed simulations
Wall lubrication	Antal [9]	
Virtual mass	Not considered	

3.3. Turbulence modelling

Due to the small density and the small scales of the dispersed gas, in the homogeneous flow regime, it suffices to consider turbulence in the continuous phase [10]. The two-equation *k-ω* Shear-Stress-Transport (SST) model was implemented to estimate the Reynolds stresses, and the Production Kato-Launder modification option was selected. The constants of the model follow their single-phase counterparts. In the present study, bubble-induced turbulence has been neglected.

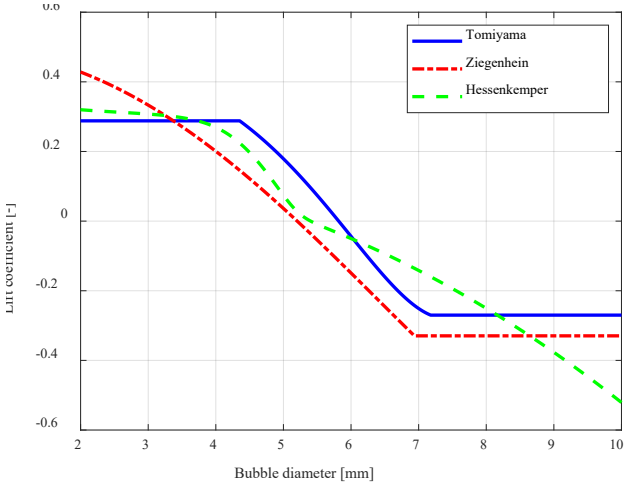

Figure 2. Lift coefficient as a function of the bubble diameter for the different lift coefficient correlations considered.

3.4. Numerical settings and boundary conditions

Transient 3D simulations are performed using the commercial code ANSYS Fluent 2021 R2, on a structured grid of 260 000 elements. Results were averaged over 60 s of flow time, to ensure that they are independent on the initial transient. The time step size was set equal to 0.001 ensuring a Courant-Friedrichs-Lewy number lower than 1. The Phase-Couple SIMPLE (PC-SIMPLE) algorithm was used for the pressure-velocity coupling. A second-order bounded Euler implicit scheme was used for the temporal discretization.

The least squares cell-based formulation and the PRESTO! discretization schemes were considered for spatial representation of gradients and pressure, respectively. In bubble columns, high order schemes are required to describe the transient nature of the flow, thus the QUICK method (third-order accuracy) was implemented for both momentum and volume fraction equations. The second-order upwind scheme was instead chosen for the turbulent quantities.

A uniform inlet was used to model the gas sparger and the gas velocity was imposed at the column inlet. The turbulent quantities were set according to Kawase [11]. A degassing boundary condition was assigned to the column outlet. Table 2 reports the cases studied.

Table 2. Cases studied.

Case	Superficial gas velocity [cm/s]	Flow regime
C1	0.38	Mono-dispersed
C2	3.44	Poly-dispersed

3.5. Phases properties

Due to the hydrostatic head, a variable air density was considered. The air density changes of ± 14% concerning a fixed value calculated at the column midpoint. The air density at the bottom and top of the column was set equal to 1.6 kg/m^3 and 1.2 km/m^3, respectively. The water properties were taken at ambient temperature and pressure.

3.6. Dispersed phase modelling

This study focuses on the homogeneous flow regime, and depending on the flow regime under investigation, a fixed mono or poly-dispersed approach has been considered.

The mono-dispersed approach considers a fixed and single value for the bubble diameter, suitable for simulating the mono-dispersed homogeneous flow regime.

Conversely, three bubble classes and three velocity groups for the gas phase are implemented in the fixed poly-dispersed approach. In this way, the different dynamics of small and large bubbles resulting from a different lift force are included in the model. The three classes implemented are:

- *the positive-lift class*. This bubble class includes bubbles with a diameter smaller than the critical diameter for the lift force change of sign and hence with a positive lift coefficient, d_{cr};
- *the zero-lift class*. This bubble class includes bubbles with diameter approximately equal to d_{cr} and hence with zero lift coefficient;
- *the negative-lift class*. This bubble class includes bubble with diameter larger than d_{cr} and hence with negative lift coefficient.

The bubble diameter for each bubble class and the mass fraction of small, medium, and large bubble classes were set according to the experimental data.

4. Results

Table 3 compares the experimental and the predicted global gas holdup. The global gas holdup, ε_{g}, is a global flow property of fundamental and practical importance as it determines the mean residence time of the dispersed gas phase inside the column. In addition, combined with the bubble size distribution, it provides the interfacial area for the heat and mass transfer rate. Therefore, a precise prediction of the global gas holdup is useful for the reactor design, optimization, and scale up.

Table 2. Cases studied.

Case	$\varepsilon_{\mathrm{g,EXP}}$ [%]	$\varepsilon_{\mathrm{g,CFD}}$ [%]	Error [%]
C1-Tomiyama	1.573	1.485	-5.59
C1-Ziegenhein	1.573	1.501	-4.60
C1-Hessenkemper	1.573	1.494	-5.02
C2- Tomiyama	16.26	15.267	-6.11
C2-Hessenkemper	16.26	14.573	-10.37

The numerical model proposed allows a correct estimation of the global gas holdup. In particular, the numerical model slightly underestimates its value, with a maximum error of -10.37 %. The underestimation of the global gas holdup can be explained by an underestimation of the drag coefficient, which results in a lower residence time of bubbles in the column and, therefore, in a lower global holdup.

Concerning case study C1, there are no significant differences between the different lift coefficient correlations, with an error always less than 10%. Figure 2 compares the numerical and experimental local gas holdup profiles. Despite being in the mono-dispersed homogeneous flow regime, the experimental profile is slightly centre-picked, whereas the numerical one is flat.

The main reason is related to the air maldistribution at the gas sparger. At low superficial gas velocity, air does not flow through all the sparger holes but only through the centre ones, influencing the local gas volume fraction profiles. This effect is typical for low volumetric flow rates where the overpressure is not enough to activate all holes equally. Since it was impossible to quantify the sparger maldistribution rigorously, it was not included in the numerical model and must be considered when interpreting the numerical results.

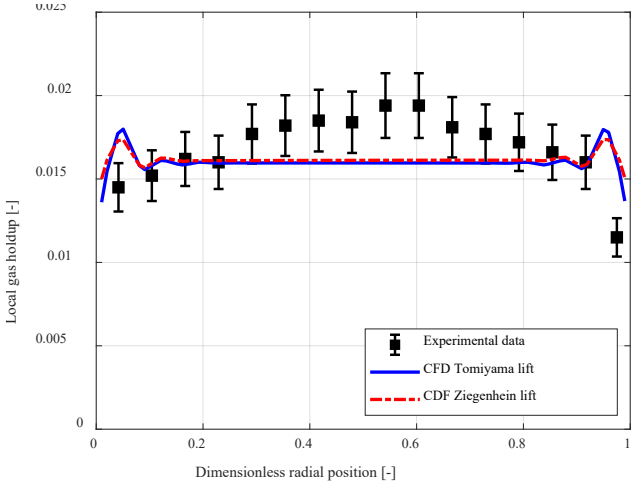

Figure 2. Comparison between experimental and numerical local gas holdup profiles. Case C1

Concerning the comparison between the different lift coefficient correlations, the Hessenkemper model provides the same results as the Ziegenhein correlation, which have not been reported in the figure for clarity. Indeed, as Figure 1 shows, the two correlations predict the same lift coefficient for the bubble diameter considered in this study (d_b =3.2 mm).

The Tomiyama et al. (2002) correlation predicts a slightly lower local gas holdup in the centre of the column, but the near-wall peaks are more pronounced. However, no remarkable differences between the three lift coefficient correlations have been found in the mono-dispersed homogeneous flow regime.

Focusing on the poly-dispersed homogeneous flow regime, the results regarding the local void fraction profile are shown in Figure 3. In particular, the Tomiyama and the Hessenkemper lift coefficient correlations have been compared.

The numerical model does not estimate the near-wall local void fraction profile correctly since it largely overestimates the void fraction near the vertical wall, resulting in a wall-picked profile.

This suggests the predominant contribution of small bubbles with respect to the experimental data. Small bubbles spread in the whole cross-section of the bubble column, limiting liquid recirculation and increasing the gas volume fraction. Indeed, by fixing the number of large bubbles and increasing the number of small bubbles, the local gas volume fraction profiles may gradually change from centre-peaked to flat to wall-peaked.

Conversely, looking at the column centre, the numerical results are in perfect agreement with the experimental data.

Concerning the comparison between the Tomiyama and Hessenkemper lift coefficient correlations, the two models provide very similar results, with the Hessenkemper correlation that perform slightly better in the near-wall region.

Several factors can explain the discrepancies between the numerical results and the experimental data. One of them is the effect of other bubbles on the lateral movement of bubbles. For example, Lift coefficient correlations in the literature were derived from considerations for an isolated bubble rising in a quiescent liquid. However, as many authors emphasized, these correlations become less appropriate as soon as the bubble is surrounded by other bubbles. Several papers in the literature have already dealt with this topic concerning the drag force, defining a swarm factor and linking it to the local or global gas volume fraction. However, a swarm effect for the lift force, however, has not yet been experimentally studied.

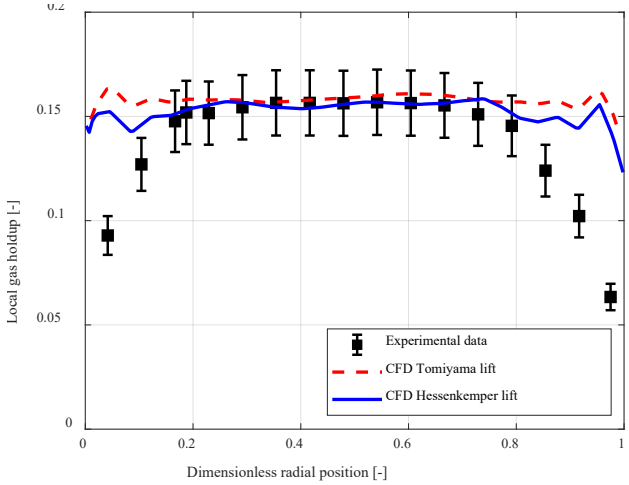

Figure 3. Comparison between experimental and numerical local gas holdup profiles. Case C2

5. Conclusions

In this study, CFD simulations of a large-scale bubble column operating the mono- and poly-dispersed homogeneous flow regime were performed. The numerical results and the experimental data concerning the global gas holdup were well-conformed. However, the CFD model did not correctly calculate the near-wall local gas holdup profile. In the mono-dispersed homogeneous flow regime, the air maldistribution at the sparger causes the air injection only at the column's centre, generating centre-picked local gas holdup profiles. In the poly-dispersed homogeneous flow regime, the reason can be related to the absence of a swarm effect acting on the lift force, which should be included in the numerical model.

Future experimental and numerical studies should focus on the motion of bubble swarms in the lateral direction to provide correlations concerning the momentum exchange between the phases accounting for the presence of other bubbles.

6. References

[1] Rollbusch P, Bothe M, Becker M, Ludwig M, Grünewald M, Schlüter M and Franke R 2015 Chem. Eng. Sci. **126** 660-678.

[2] Besagni G 2021 *Chin. J. Chem.* Eng. **40** 48-52.

[3] Besagni G 2021 *Int. J. Multiph. Flow* **135** 103510.

[4] Tomiyama A 1998 Multiph. Sci. Techenol. **10** 369-405.

[5] Tomiyama A, Tamai H, Zun S and Hosokawa 2002 *Chem. Eng. Sci.* **57** 1849-1858.

[6] Ziegenhein T, Tomiyama A and Lucas D 2018 *Int. J. Multiph. Flow* 108 11-24.

[7] Hessenkemper H, Ziegenhein T, Rzehak R, Lucas D and Tomiyama A 2021 *Int. J. Multiph. Flow* **138** 103587.

[8] Burns A D, Frank T, Hamill I, Shi J M 2004 *5th international conference on multiphase flow ICMF* 4 1-17.

[9] Antal S P, Lahey Jr and Flaherty J E 1991 *Int. J. Multiph. Flow* **5** 635-652.

[10] Rzehak R and Krepper E 2013 *Nucl. Eng. Des.* **265** 701-711.

[11] Kawase Y and Moo-Young M 1989 *Chem. Eng. J.* **40** 55-58